Polymer 54 (2013) 1820–1831

Contents lists available at SciVerse ScienceDirect

Polymer

journal homepage: www.elsevier.com/locate/polymer

Electrochromic polyaniline/graphite oxide nanocomposites with endured electrochemical energy storage

Huige Wei [a,b], Jiahua Zhu [a], Shijie Wu [c], Suying Wei [b,**], Zhanhu Guo [a,*]

[a] Integrated Composites Laboratory (ICL), Dan F. Smith Department of Chemical Engineering, Lamar University, Beaumont, TX 77710, USA
[b] Department of Chemistry and Biochemistry, Lamar University, Beaumont, TX 77710, USA
[c] Agilent Technologies, Inc., Chandler, AZ 85226, USA

ARTICLE INFO

Article history:
Received 4 December 2012
Received in revised form
28 December 2012
Accepted 19 January 2013
Available online 8 February 2013

Keywords:
Polyaniline nanocomposite film
Electropolymerization
Electrochromism

ABSTRACT

Polyaniline (PANI)/graphite oxide (GO) nanocomposite films were fabricated by electropolymerization of aniline monomers onto GO coated indium tin oxide (ITO) glass slides, which were prepared by spin coating technique. The morphology as well as the crystalline structure of the composite films were studied using Fourier transform infrared spectroscopy (FT-IR), atomic force microscopy (AFM), and X-ray diffraction (XRD). The results confirm the obtained composite structural films and the interactions between the polymer matrix and the GO particles. The optical properties and the electrochemical capacitive behaviors of the composite films for electrochromic displays and electrochemical energy storage devices applications were investigated using the spectroelectrochemistry (SEC), cyclic voltammetry (CV) and galvanostatic charge–discharge measurements. The composite films show multi-color electrochromism at different potentials arising from PANI. A coloration efficiency of 59.3 $cm^2\ C^{-1}$ is obtained for the composite film, higher than that of the pure PANI thin films, 50.0 $cm^2\ C^{-1}$. An areal capacitance of 25.7 mF cm^{-2} that is comparable to PANI (75.1 mF cm^{-2}) is derived from the CV at a scan rate of 5 mV/s with a broader working potential window of 1.3 V. The cyclic stability studies reveal that the composite films exhibits much more enhanced durability and retains 53.1% of the capacitance even after 1000 charge–discharge galvanostatic cycles. However, the pure PANI thin films lose almost most of the charge storage or discharge capacity even after 350 cycles. The interactions between PANI matrix and GO particles are believed to be responsible for the observed enhanced stability in the nanocomposite films.

1. Introduction

The development of sustainable and renewable energy storage resources with both high power density and large energy density has received significant attention due to the depletion of fossil fuels and climate change [1–3]. The electrochemical capacitors have been under extensive study for applications for future systems including portable electronics, hybrid electric vehicles, and large industrial equipments owing to their advantages of high energy and power density as well as long cycle life [4,5]. The electrochemical capacitors are expected to have promising potentials for filling the gap between the batteries and the conventional electrostatic capacitors [6].

Two types of electrochemical capacitors have been proposed based on different charge storage mechanisms [7]. The first one is non-Faradic, where only ion adsorption takes place between the interfaces of electrodes and electrolyte. The capacitors of this type are called electric double layer capacitors (EDLCs), or ultracapacitors. EDLCs are mainly fabricated from carbon materials with large specific surface area (SSA), i.e., activated carbons (ACs) [8], carbon nanofibers [9] or nanotubes [10], ordered mesoporous carbons (OMCs) [11], and graphene nanosheets (GNS) [12,13]. EDLCs have the advantage of high power density (>10 kW kg^{-1}) and long cycle life (>10^6 cycles) [14]. However, low energy density (<5 kh/kg) [6,15] and much lower areal capacitance (capacitance per unit area) ranging from 10 to 40 μF cm^{-2} due to both low density and gravimetric capacitance (capacitance per unit mass) of carbon remain the challenges. The other type of electrochemical capacitors, pseudocapacitors or supercapacitors, is based on Faradic process, where the energy storage is achieved by electron transfer that follows reduction–oxidation (redox) reactions in the material. The transition metal oxides including MnO_2 [16], RuO_2 [17], MoO_3 [18], Co_3O_4 [19] and VO_x [20], and electrically conducting polymers (CPs) such as polythiophenes (PThs) [21], polypyrrole [22,23],

* Corresponding author. Tel.: +1 409 880 7654; fax: +1 409 880 2197.
** Corresponding author. Tel.: +1 409 880 7976; fax: +1 409 880 8270.
E-mail addresses: suying.wei@lamar.edu (S. Wei), zhanhu.guo@lamar.edu (Z. Guo).

0032-3861/$ – see front matter © 2013 Elsevier Ltd. All rights reserved.
http://dx.doi.org/10.1016/j.polymer.2013.01.051

poly(DNTD) [24,25], and polyaniline (PANI) [26] can be utilized for designing electrochemical capacitors of this type. The problem with respect to the transition metals is their relative high electrical resistance, which gives rise to lower power density. CPs have relative high conductivity and low cost compared to the carbon-based electrode materials. More importantly, CPs possess much higher gravimetric capacitance via pseudocapacitive redox reactions and much larger density, rendering them possible to increase the areal capacitance while keeping similar or even thinner films as those of the conventional carbon-based material. However, mechanical degradation of the electrode and fading electrochemical performance caused by the swelling and shrinking during the cycling redox reactions of CPs impose limitations on their applications as electrochemical capacitors [27].

For applications such as small scale electronics and stationary energy storage devices where areal capacitance is a better indicator of the supercapacitor performance than gravimetric capacitance, although the gravimetric capacitance has always been used in the literature for comparison of the supercapacitor performance [28,29], a strategy of combining a Faradaic pesudocapacitive conjugated polymers and EDLs systems has been developed to obtain electrochemical capacitors with desirable properties. Among the various CPs, PANI has received special attention because of its intriguing properties such as facile polymerization in aqueous media [30–33] or non-aqueous media [34], good stability in air, low cost, and high conductivity. Specially, high pseudocapacitance arising from the versatile redox reactions and corresponding color changes make PANI promising candidate for electrochemical capacitors [35,36] and electrochromic (EC) applications [37,38].

Graphite oxide (GO), derived from chemically modified graphene, has attracted great interest owing to its many advantages, such as low manufacturing cost, facile mass production, and remarkable mechanical behaviors [39]. GO can be easily exfoliated into single sheets under sonication and serves as a promising starting material for the production of functional composite materials given a large number of oxygen-containing functional groups in-plane and out-of-plane that provide sufficient defects and potential functionalization [40]. Some efforts have been made to investigate the capacitative properties of GO composites incorporated with PANI [41], polypyrrole (PPy) [42], or poly(sodium 4-styrensulfonate) [43]. However, a comprehensive study of the electrochromic behaviors and the electrochemical energy storage of these nanocomposite films, to the best of our knowledge, has not been reported yet [40].

In this work, the PANI/GO nanocomposite thin films were prepared by a facile method, in which aniline monomers in sulfuric acid solutions were electrodeposited onto GO coated indium tin oxide (ITO) glass slides, which were prepared by spin coating technique. The composition and morphology as well as the structure of the composite films were studied using Fourier transform infrared spectroscopy (FT-IR), atomic force microscopy (AFM), and X-ray diffraction (XRD). The optical properties and capacity behaviors of the composite films for electrochromic (EC) and energy storage devices applications were investigated using spectroelectrochemistry (SEC), cyclic voltammetry (CV) and galvanostatic charge–discharge measurements.

2. Experimental

2.1. Materials

Natural graphite powder (SP-1) was purchased from Bay Carbon Inc, USA. Aniline (C_6H_7N, ≥99.0%), sulfuric acid (H_2SO_4, 95.0%–98.0%), hydrochloric acid (HCl, 36.5–38.0%), potassium persulfate ($K_2S_2O_8$, ≥99.0%), phosphorus pentoxide (P_2O_5, ≥98.0%), potassium permanganate ($KMnO_4$, ≥99.0%), H_2O_2 solution (PERDROGEN® 30% H_2O_2 (w/w)), polyvinylidene fluoride (PVDF) powder (Mw ≈ 534,000), and PVDF membrane filters (Durapore® PVDF) were all purchased from Sigma Aldrich. The microscope glass slides and indium tin oxide (ITO) coated glass slides were provided by Fisher and NanoSci Inc, respectively. ITO coated glass slides were sonicated in ethanol for 10 min, and then immersed in an aqueous solution containing 4 mL 28.86 wt% ammonium hydroxide, 4 mL 30.0 wt% hydrogen peroxide (both from Fisher) and 20 mL deionized water for 10 min, and sonicated in deionized water for 10 min before usage.

2.2. Synthesis of graphite oxide

The graphite oxide (GO) was obtained from exfoliation of chemically treated graphite with the aid of ultrasonication. Graphite oxide was synthesized following the modified Hummers' method [44,45] using natural graphite powders as the starting material. Specifically, a pre-oxidation of the graphite was performed before the graphite oxide preparation according to Hummers' method, which was essentially important for producing completely oxidized products. In the work, 3.0 g graphite powders were put into an 80 °C solution containing 12 mL concentrated H_2SO_4, 4.0 g $K_2S_2O_8$, and 4.0 g P_2O_5. The resultant dark blue mixture was thermally isolated and allowed to cool down to room temperature over a period of 6 h. Then, the mixture was diluted carefully using distilled water, filtered, and washed with a PVDF membrane until to neutral pH. The obtained preoxidized graphite was dried in air at ambient temperature overnight and then was subjected to oxidation by Hummers' method. Briefly, the oxidized graphite powders were dispersed in 120 mL concentrated H_2SO_4 at 0 °C. 15.0 g $KMnO_4$ was added gradually with stirring and cooling. The temperature of the mixture was not allowed to reach or higher than 20 °C. The mixture was then stirred at 35 °C for 2 h with 250 mL distilled water added. The reaction was terminated after 15 min by adding a large amount of distilled water (about 700 mL) and 20 mL H_2O_2 solution. The bright yellow reactant mixture was then filtered and washed with 1:10 HCl solution (1 L) to remove metal ions. The product was suspended in distilled water to give a viscous, brown, 2.0 wt% dispersion, which was subjected to dialysis to completely remove metal ions and acids. The final concentration of the graphite oxide solution was 1.4 wt% determined by thermogravimetric analysis (TGA). The solution was further diluted to 0.5 wt% for spin coating.

2.3. Preparation of PANI/GO thin film electrodes

The GO transparent film was prepared by drop casting about 2 mL 0.5 wt% GO dispersion onto the ITO glass and kept at 2000 rpm for 20 s. The film was naturally dried in air overnight before the electropolymerization. The electropolymerization of aniline onto GO film was performed on an electrochemical working station VersaSTAT 4 potentiostat (Princeton Applied Research) in air. A typical electrochemical cell consisting of a reference electrode, a working electrode, and a counter electrode was employed. An Ag/AgCl electrode saturated with KCl served as the reference electrode and a platinum (Pt) wire as the counter electrode. The GO coated ITO glass slide with an effective area of 5 cm^2 served as the working electrode. A long pathlength home-made spectroelectrochemical cell with Teflon cell body with front and rear windows clapped with two steel plates was used when the ITO glass slide was used as the working electrode for optical characterizations. A typical electrochemical polymerization was performed 30 cycles scanned back and forth from 0 to +1.3 V vs. Ag/AgCl at a scan rate of 50 mV/s in 0.5 M H_2SO_4 aqueous solution containing 0.1 M aniline.

2.4. Characterizations

The morphology of the thin films grown on the ITO glass slides was characterized by atomic force microscopy (AFM, Agilent 5600 system with multipurpose 90 μm scanner. Imaging of AFM was done in acoustic ac mode (AAC) using a silicon tip with a force constant of 2.8 N/m and a resonance frequency of 70 kHz. FT-IR spectrometer coupled with an ATR accessory (Bruker Inc. Vector 22) was used to characterize the surface functionality of the thin films grown on the ITO glass slides in the range of 4000 to 500 cm^{-1} at a resolution of 4 cm^{-1}. X-ray diffraction (XRD) analysis was carried out with a Bruker AXS D8 Discover diffractometer with GADDS (General Area Detector Diffraction System) operating with a Cu-Kα radiation source filtered with a graphite monochromator ($\lambda = 1.5406$ Å). Data were collected in a range of 5 to 80°.

The electrochemical properties of the GO film, pure PANI film, and PANI/GO nanocomposite film were investigated by CV scanned from −0.5 to 0.8 V vs. Ag/AgCl at a scan rate of 10 mV/s in 0.5 M H_2SO_4 aqueous solution. The electrochemical impedance spectroscopy (EIS) was carried out in the frequency range of 100,000–0.01 Hz at a 10 mV amplitude referring to the open circuit potential. The spectroelectrochemistry measurements were performed on a Jasco V-670 spectrophotometer coupled with the potentiostat for applying electrochemical potentials. The *In situ* chronocoulometry (CC) were conducted under a square-wave voltage of 0.8 and −0.2 V with a pulse width of 20 s. All the characterizations were carried out in air.

The electrochemical energy storing behaviors of the films were studied by CV at a series of scan rates and galvanostatic charge–discharge measurements in 0.5 M H_2SO_4 aqueous solution. The endurance of the composite films was also assessed using charge–discharge measurements at a current density of 3 mA cm^{-2} for 1000 cycles.

3. Results and discussion

3.1. Synthesis of PANI/GO hybrid films

Fig. 1(a, b) shows the cyclic voltammogram (CV) obtained during the potentiodynamic electropolymerization growth of PANI onto bare and GO coated ITO glass slide, respectively. The pure PANI film and PANI/GO nanocomposite film were prepared by sweeping the potential between 0 and +1.3 V at a scan rate of 50 mV s^{-1} in an aqueous solution containing 0.1 M aniline and 0.5 M H_2SO_4. The film growth can be verified by the increased current with increasing the CV cycles. These two films exhibit similar CV patterns except of lower anodic current peaks observed for the PANI/GO composite film growth, which is attributed to the increased

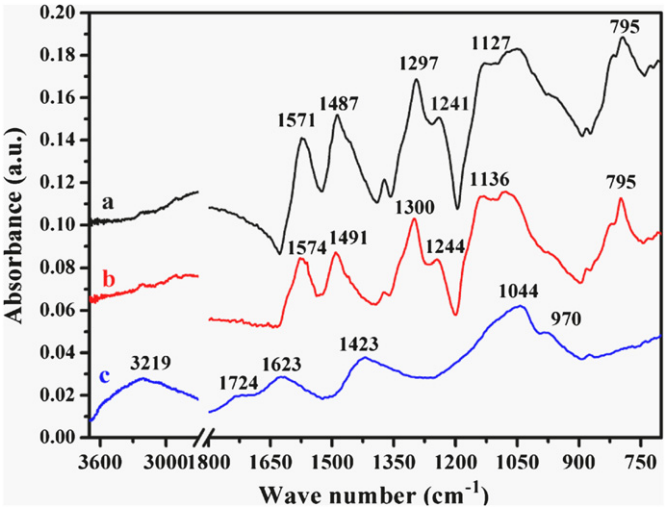

Fig. 2. FT-TR spectra of the (a) PANI film, (b) PANI/GO nanocomposite film, and (c) GO film, respectively.

resistance of the GO film on the ITO. It's interesting that, for the nanocomposite film, the anodic irreversible peak starting at around +0.9 V, which corresponds to the oxidation of aniline monomers and the initiation of the electropolymerization of PANI [46], is not so remarkable as that of pure PANI film upon closer observation. Besides the GO induced larger resistance, this phenomenon is probably explained by the reduced electron density on nitrogen atoms caused by the hydrogen bonding formed between the carboxylic groups located at the edges of GO and the amine groups of aniline monomers. These voltammograms on ITO were different from the CVs usually obtained by electropolymerization of PANI on platinum electrodes that commonly exhibit well-defined redox peaks corresponding to a series of redox transitions: oxidation of the fully reduced insulating form (leucoemerladine) to its radical cation (polaron, emeraldine), followed by the oxidation of degradation products and/or intermediate species, and finally the transition from the delocalized polaronic state to a localized bipolaron or quinoid form (pernigraniline) [47]. The reason for different voltammogram behaviors between the films on indium tin oxide and Pt electrodes might lie in the conductivity difference of the substrates that renders the electropolymerization easier on Pt than on ITO substrates [48–50].

The mass of monomers electropolymerized onto the substrate can be roughly estimated from the total Faradic charges consumed in the electropolymerization assuming an average of 2.5 electrons per aniline monomer in emeraldine [51,52].

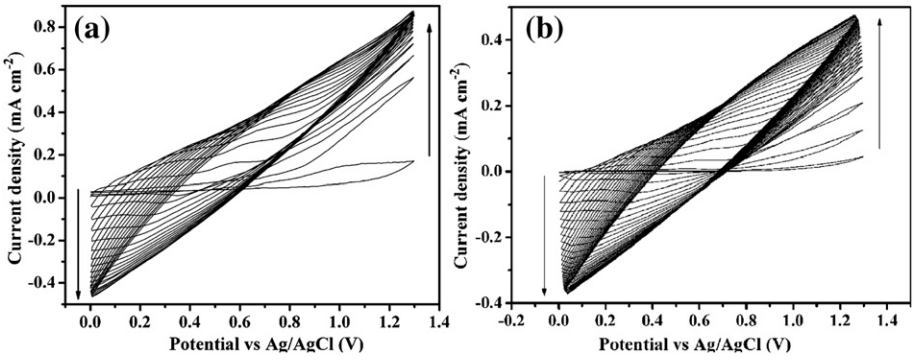

Fig. 1. Electropolymerization synthesis of PANI onto (a) bare and (b) GO coated ITO glass at a scan rate of 50 mV/s in 0.5 M H_2SO_4 aqueous solution containing 0.1 M aniline.

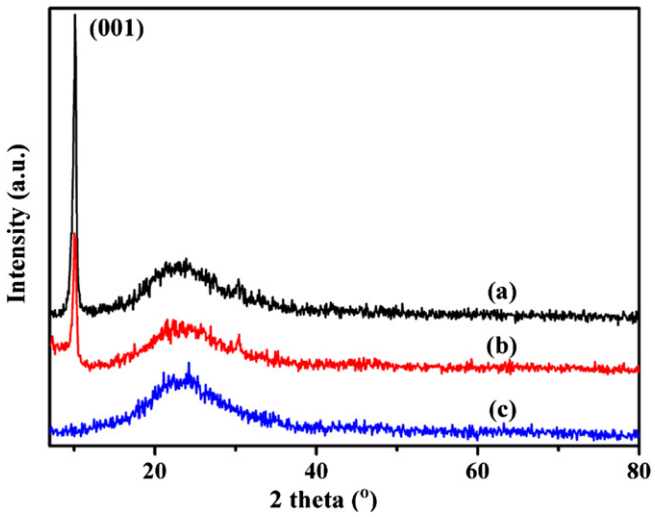

Fig. 3. XRD patterns of the (a) GO film, (b) PANI/GO nanocomposite film, and (c) PANI film, respectively.

$$m = \frac{CM_m}{2.5F} \tag{1}$$

where m is the mass of PANI polymerized onto the substrate, g; C is the total Faradic charges consumed in the electropolymerization, C, M_m is molecular mass of aniline monomer (93.13 g/mol), and F is Faraday constant (96,485 C/mol). Therefore, about 14.4 and 6.8 μg polymers were obtained for pure PANI and PANI/GO composite films, respectively, using Equation (1).

3.2. Morphology and composition analysis

Fig. 2(a–c) shows the FT-IR spectra of the PANI film, PANI/GO composite film, and GO film in the region of 4000-500 cm^{-1}, respectively. In Fig. 2(c), the FT-IR spectrum of GO shows a broad spectra around 3219 cm^{-1}, which originates from the stretching vibrations of the –OH group in the GO [53]. The peak at 1724 cm^{-1} arises from the C=O stretching vibrations from the carbonyl and carboxylic groups [54]. The band at 1623 cm^{-1} is attributed to the aromatic C=C stretching, and the bands at 1423 and 1044 cm^{-1} correspond to the carboxy C-O and alkoxy C-O groups [55,56]. For the PANI thin film onto ITO using multiple CV methods, Fig. 2(a), the peaks at 1571 and 1487 cm^{-1} correspond to the characteristic C=C stretching mode of the quinoid and benzenoid rings, respectively [57]. The peaks at 1127 and 795 cm^{-1} are assigned to the in-plane and out-of-plane bending of the C–H [58,59]. The peaks at 1297 and 1235 cm^{-1} are attributed to the C–N and C=N stretching mode [60,61]. The PANI/GO composite film mainly shows the characteristic peaks of the polymer matrix, as shown in Fig. 2(b). It should be noted that the peaks corresponding to the quinoid and benzenoid rings, respectively, of the PANI matrix in the composite film shift to higher wavenumbers and the intensity ratio is different from that of pure PANI. The interactions including π–π stacking, electrostatic interactions, and hydrogen bonding existing between GO and PANI [62], are believed to cause the spectrum changes.

Fig. 3(a–c) shows the XRD pattern of the films. An intense, sharp peak centered at $2\theta = 10.07°$ of (001) plane for the stacked GO sample after the drying process, corresponds to the inter planar spacing of 0.88 nm of GO sheets using Bragg's law:

$$d = \frac{\lambda}{2d\sin\theta} \tag{2}$$

where λ is 1.5406 Å for the wavelength of Cu–Ka radiation, and θ is the Bragg angle. The average grain size (L) was estimated from the Debye–Scherrer Equation (3) [63]:

$$L = \frac{K\cdot\lambda}{\beta(2\theta)\cdot\cos(\theta)} \tag{3}$$

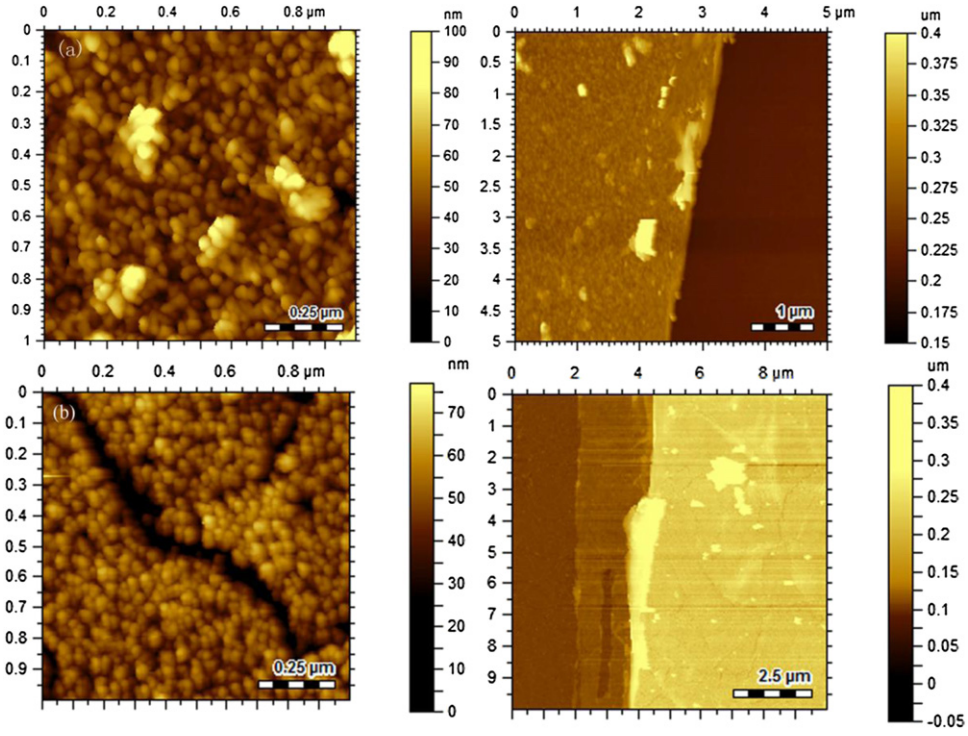

Fig. 4. AFM images (left) and section profiles (right) of the (a) PANI film, and (b) PANI/GO nanocomposite film onto ITO glass, respectively.

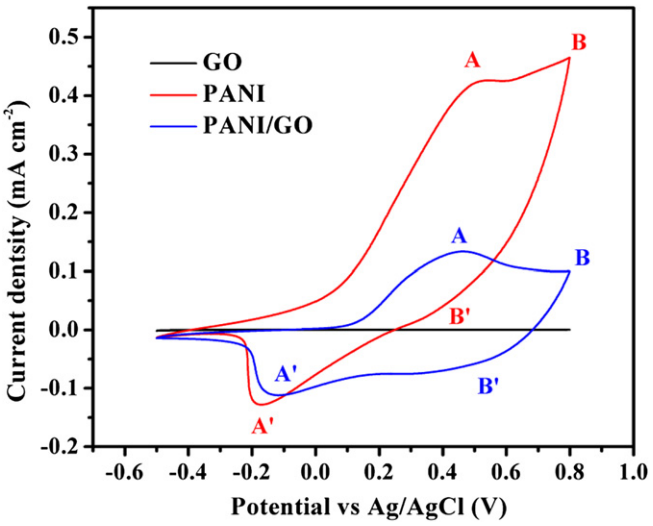

Fig. 5. CV curves of the GO film, PANI film, and PANI/GO nanocomposite film onto ITO in 0.5 M H_2SO_4 at a scan rate of 10 mV/s.

where $\beta(2\theta)$ is the full width at half-maximum (FWHM), K is the shape factor depending on the miller index of the reflecting plane and the shape of the crystal. If the shape is unknown, K is often assigned a value of 0.9 [64]. The peaks at $2\theta = 10.04°$ were used to estimate the grain size of GO to give 5.1 nm for GO. Another peak centered at 22.8° corresponds to the (002) of graphite [65]. For PANI film, a broad band extending from 15 to 34° is ascribed to crystallized PANI [66]. The intensity of the peak at 10.04° is attenuated in the composite film, which is caused by the PANI matrix. Therefore, the XRD result confirms the presence of the polymer and GO in the composite film.

Fig. 4 shows the AFM surface topography of the films on the left part, and the thickness of the films can be measured by large scans of section profiles on the right part. The composite film displays a uniform structure. The thickness of pure PANI film and the nanocomposite film on ITO is measured to be 80 and 125 nm, respectively. The increased thickness of the PANI/GO film compared to that of PANI is attributed to the thickness of GO substrate though less polymer was electropolymerized onto GO coated ITO.

3.3. Electrochemical and optical properties

3.3.1. Cyclic voltammetry

The cyclic voltammograms of the films grown on the ITO coated glass slides were recorded in 0.5 M H_2SO_4 aqueous solution at a scan rate of 10 mV/s from −0.5 to 0.8 V. Fig. 5 shows the CV of the GO film, PANI film and PANI/GO nanocomposite film, respectively. No obvious peaks were observed in the GO film. For the PANI film, two redox pairs, B/B′ and C/C′ originating from the transitions between leucoemeraldine salt (LS) to emeraldine salt (ES) and emeraldine salt (ES) to pernigraniline salt (PS) of PANI, indicate the typical pseudocapacitance characteristic of the materials [67,68]. Peak potential separation has been used to determine the reversibility of an electrochemical redox reaction. Generally speaking, smaller peak potential separation usually relates to a reversible reaction, while larger peak potential separation is often observed in irreversible reactions [69]. It's worth noting that the potential difference between A and A′, and the potential difference B and B′ of the nanocomposite film are smaller than those of the pure PANI film, indicating a better reversibility of the redox reactions in the composite film.

3.3.2. Spectroelectrochemistry of GO, PANI, and PANI/GO composite films

Fig. 6(a, b) shows the UV-Vis transmission spectra of the PANI film, and PANI/GO nanocomposite film at different potentials, respectively. At positive potentials, i.e., 0.8 V, a characteristic absorbance band distinguished around 750 nm is attributed to $\pi-\pi^*$ transition in the quinoid ring of the polyaniline polymer in pure PANI and its GO nanocomposite films [70]. Correspondingly, varying colors of the composite film were observed upon different potentials. The composite film displayed light yellow at −0.2 V (reduced state), light green at 0.5 V, blue at 0.8 V (partially oxidized state), and finally dark blue at 1.0 V (fully oxidized state). Fig. 7 shows the digital photograph of color switching at different potentials in 0.5 M H_2SO_4. The pictures were taken after applying different potentials on the film for 20 s.

The coloration switching response of the films is also studied by applying potential steps of 0.8 and −0.2 V with a pulse width of 20 s. Fig. 8 shows the transmittance-time and corresponding charge density–time curves at 633 nm under an alternative square-wave voltage of 0.8 and −0.2 V. A transmittance modulation (transmittance difference in the bleached and colored states in EC materials) of 37.4 and 60.6% are calculated for the PANI film and the PANI/GO nanocomposite film, respectively. The coloration time (τ_c) and bleaching time (τ_b) are defined as the time required for a 90% change in the full transmittance modulation, respectively [71]. For PANI, τ_b is found to be 9.5 s and τ_c is 13.7 s from the first cycle in the transmittance-time curve, Fig. 8 (left pat), and the composite film shows a bleaching time of 15.8 s and nearly the same coloration time of 15.3 s. The phenomenon that GO substrate has more noticeable effect on the τ_b of the polymer matrix is inferred to arise from the affinity of the oxygen functionality on GO [72] with hydrogen ejected from the polymer during the bleaching kinetics.

Coloration efficiency (CE or η), which is defined as the change in optical density (OD) per unit charge (Q) inserted into (or extracted from) the EC films, i.e., the amount of energy to affect a color

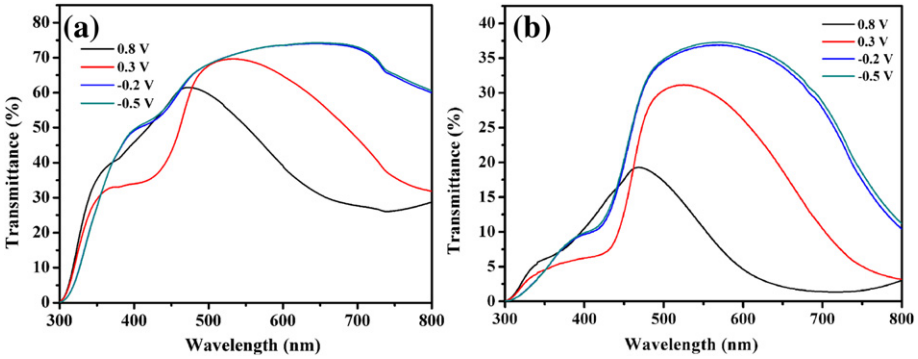

Fig. 6. UV-Vis spectra of the (a) PANI film and (b) PANI/GO nanocomposite film onto ITO in 0.5 M H_2SO_4 aqueous solution at different potentials.

Fig. 7. Digital photograph of color switching of the PANI/GO nanocomposite film onto ITO at different potentials in 0.5 M H_2SO_4.

change, is an important consideration for the practical applications of EC materials in the display and window devices. The CE can be calculated from Equations (4) and (5) [73]:

$$\eta = \Delta OD(\lambda)/Q_d \quad (4)$$

$$\Delta OD = \log[T_{colored}/T_{bleached}] \quad (5)$$

where ΔOD is the change in optical density, λ is the dominant wavelength for the material, Q_d is the charge density (injected/ejected charges per unit electrode area), and $T_{bleached}$ refers to the transmittance of the film in the bleached state, and $T_{colored}$ refers to the varying transmittance of the film during the coloring process [26]. Fig. 9 shows the plots of the calculated ΔOD obtained from the first cycle in the transmittance-time curve, Fig. 8 (left part), at a wavelength of 633 nm versus the corresponding inserted charge density obtained from charge density–time curve, Fig. 8 (right part). The CE (η) is extracted as the slope of the line fitting to the linear region of the curve. The values of CE are found to be 50.0 and 59.3 $cm^2\ C^{-1}$ for the PANI film and the PANI/GO nanocomposite film, respectively. Interestingly, a higher CE is obtained for the composite film, indicating a greater optical density change caused by fewer charges injected/ejected.

3.4. Capacitive performance for energy storage applications

3.4.1. Electrochemical impedance spectroscopy (EIS)

EIS was employed to investigate the inner resistance of the films and their capacitance properties [74]. Fig. 10(a–c) shows the Nyquist plots of the GO film, PANI film, and PANI/GO composite film onto ITO glass, respectively. The GO film exhibits a semicircle at higher frequency region, inset of Fig. 10(a), corresponding to an electron-transfer-limited process [75] while no or negligible semicircle observed in the diagrams of the PANI film or the PANI/GO composite films. The results show that the interactions between PANI and GO could greatly improve the charge-transfer reactions for the composite film. The inner resistance, or equivalent series resistance (ESR), which mainly arises from the electrolyte, the intrinsic resistance of the active material, and the contact resistance at the active material/current collector interface [76], is approximately 148, 22 and 246 Ω for the GO film, PANI film, and PANI/GO composite film, respectively, which is obtained from the

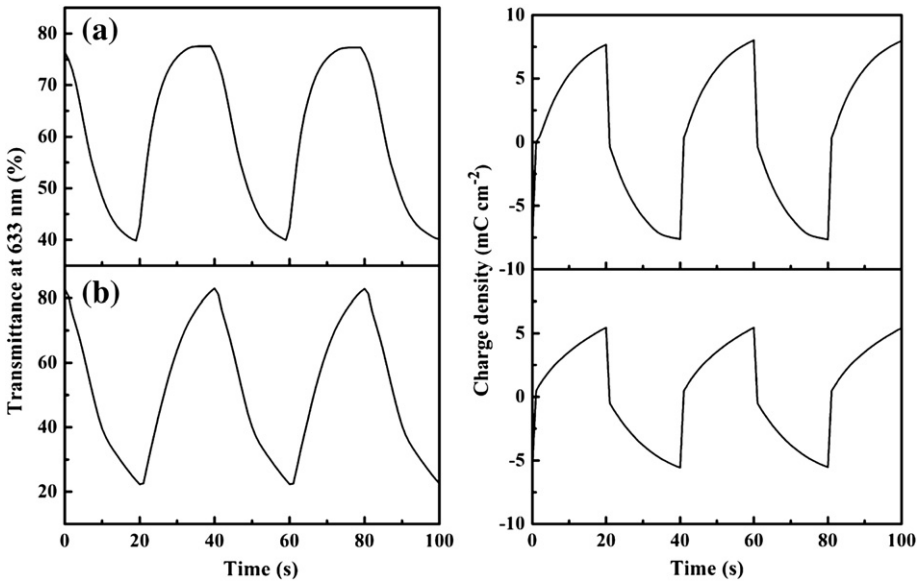

Fig. 8. *In situ* corresponding transmittance (left) and chronocoulometry (right) of the (a) PANI and (b) PANI/GO nanocomposite film onto ITO at 633 nm in 0.5 M H_2SO_4 aqueous solution. The tests were conducted under a square-wave voltage of 0.8 and −0.2 V with a pulse width of 20 s.

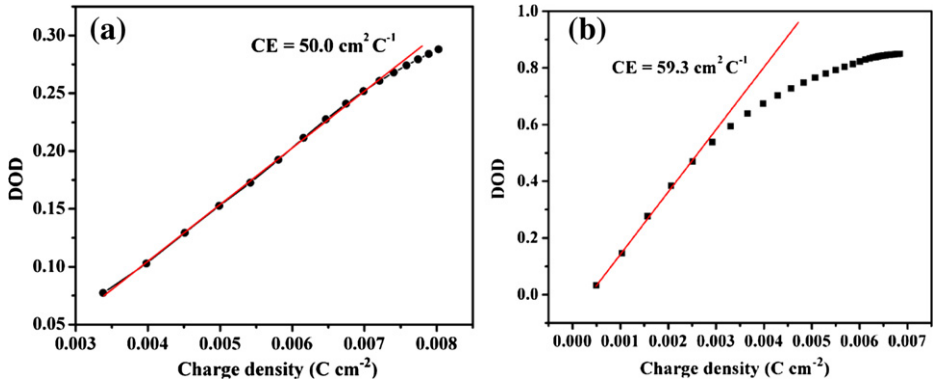

Fig. 9. The plot of *in situ* optical density (ΔOD) versus charge density of the (a) PANI film and (b) PANI/GO nanocomposite film. The optical density was measured at 633 nm at 0.8 V in 0.5 M H_2SO_4 aqueous solution.

intersection of the curve at the *X*-axis [77]. Considering the same concentration of the electrolyte used, it can be inferred that PANI imposes little resistance to the composite film, and GO contributes primarily to the inner resistance. The Warburg resistance (diffusion impedance), that is, the 45° portion of the curve, results from the frequency dependent ion diffusion/transport in the electrolyte [78]. Compared to the pure PANI film, the PANI/GO composite film exhibits a shorter 45° portion, indicating an enhanced ion transport to the inner electrolyte for the composite film [79]. More importantly, the EIS plot of the composite film tends towards a more vertical line than that of the PANI film in the low frequency range with the imaginary part of the impedance increasing rapidly, characteristic of a better capacitive behavior [36]. The knee frequency, lower than which the supercapacitors begin to exhibit capacitive behavior, is of critical importance to evaluate the frequency dependence of a capacitor [80]. The knee frequency for the composite film is 0.2 Hz, indicating that PANI/GO film is more suitable than the PANI film or GO film for the supercapacitor applications.

3.4.2. *Capacitance evaluations of GO, PANI, and PANI/GO composite films*

The areal capacitance of the films was calculated from CV curves at different scan rates from −0.5 to 0.8 V in 0.5 M H_2SO_4 aqueous solution using Equation (6): [81]

$$C_S = \left(2\int i dV\right) \Big/ (S \times \Delta V \times \nu) \tag{6}$$

where C_S is the areal capacitance in F cm^{-2}, $\int i dV$ is the integrated area of the CV curve, S is the surface area of active materials in the single electrode in cm^2, ΔV is the scanned potential window in V, and ν is the scan rate in V/s.

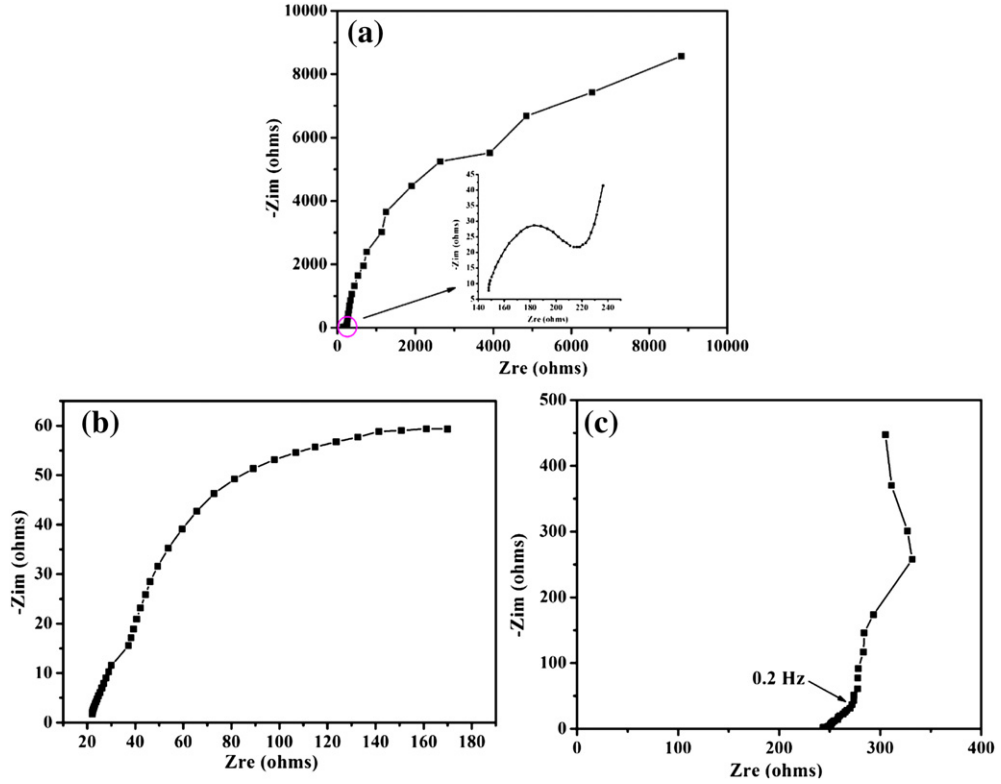

Fig. 10. Electrochemical impedance spectroscopy (Nyquist plots) of the (a) GO film, (b) PANI film and (c) PANI/GO nanocomposite film, respectively, onto ITO in 0.5 M H_2SO_4 with a frequency loop from 100 kHz to 10 mHz using a perturbation amplitude of 10 mV at the open potential.

Fig. 11(a–c) depicts the CV curves and capacitance dependence on the scan rate of the GO film, PANI film, and PANI/GO nanocomposite film, respectively. At a low scan rate of 5 mV/s, the areal capacitance of the composite film is 25 mF cm^{-2}, much higher than that of the GO film (0.14 mF cm^{-2}), and is in the same order as that of the PANI film (75 mF cm^{-2}). The areal capacitance of the composite film is higher than that has been reported for pure PANI (17 mF cm^{-2}) at the same scan rate at a lower potential window of 1.0 V synthesized from dilute polymerization process [81]. Even at a fast scan rate of 100 mV/s, the film could still deliver 9 mF cm^{-2}, while the capacitance is 0.08 and 12 mF cm^{-2} for the GO film and PANI film, respectively. The capacitance decayed with increasing the scan rate, which is caused by the relatively slow diffusion of the ions in the electrolyte to meet the need of ions near the electrode/electrolyte interface at higher scan rates [82]. The composite film can retain 28.7% of the capacitance even at higher scan rate, compared to 16.5% for the pure PANI film, indicating a better ion diffusion in the composite film, which is in good agreement with the smaller Warburg resistance confirmed by EIS measurement, Fig. 10(c). It should be noted that the areal capacitance of the PANI film is higher than that of the composite film. This phenomenon can be explained by the fact of more aniline monomers electrodeposited onto the bare ITO thus producing a thicker PANI film than the composite film [83], as confirmed by CV synthesis results.

The galvanostatic charge–discharge measurements by chronopotentiometry (CP) were also carried out on the films in 0.5 M H_2SO_4 aqueous solution to evaluate the areal capacitance of the films using Equation (7): [81]

$$C_s = (2 \times i \times t)/(S \times \Delta V) \quad (7)$$

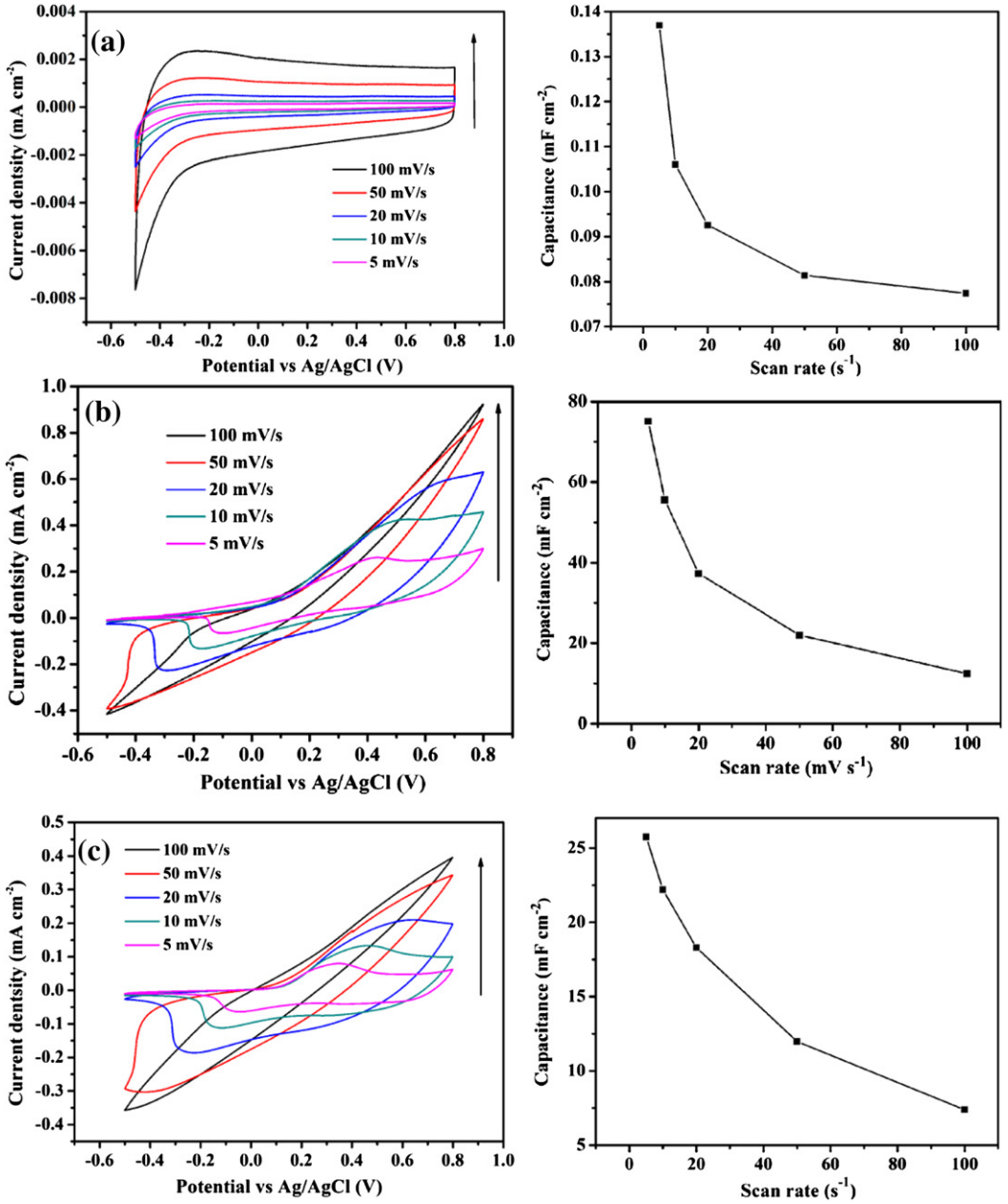

Fig. 11. CV curves (left) and scan rate dependent areal capacitance (right) of the (a) GO film, (b) PANI film, and (c) PANI/GO nanocomposite film at different scan rates under a potential range from −0.5 to 0.8 V in 0.5 M H_2SO_4 aqueous solution.

where C_s is the areal capacitance in F cm^{-2}, i is the discharge current in A, t is the discharge time in s, S is the surface area of the active materials in the single electrode in cm^2, ΔV is the scanned potential window (excluding IR drop in the beginning of the discharge) in V. Fig. 12(a–c) shows the potential responses of the films under different currents and the current density dependent areal capacitance of the films. The composite film turned to blue when fully charged to 0.8 V and gradually changed into yellow green at −0.2 V when fully discharged. Therefore, the electrochromism could be used as an interesting indicator for the capacitor applications. The GO film exhibits a triangular shape charge/discharge curve, implying that its capacitance is mainly attributed to pure electric double layer (EDL) capacitance, in which the capacitance arises from the charge separation at the electrode/electrolyte interface [79]. However, the areal capacitance of the GO film is rather low. Even at a lower current density of 0.008 mA cm^{-2}, the areal capacitance is only 0.0265 mF cm^{-2}. The areal capacitance of the composite film is enhanced significantly, reaching 19.2 mF cm^{-2} at a low current density of 0.008 mA cm^{-2} and retains 32.8% of the capacitance at a high current density of 0.16 mA cm^{-2}, about 6.3 mF cm^{-2}. The capacitance mainly arises from the faradic reactions of the polymers occurring at the electrode/electrolyte interface. For PANI, only capacitances at higher current densities can be obtained. When the current density was lowered to 0.008 mA cm^{-2}, a significant degradation of PANI occurred and cracks were observed before the film was fully discharged. These observed results are consistent with the reported poor electrochemical stability of PANI [84]. In the nanocomposite film, the GO acts as the frame-works for preventing the polymer matrix from severely swelling and shrinking during cycling [79].

The areal energy and power density are usually employed for evaluating thin film micro-batteries since the comparison has no

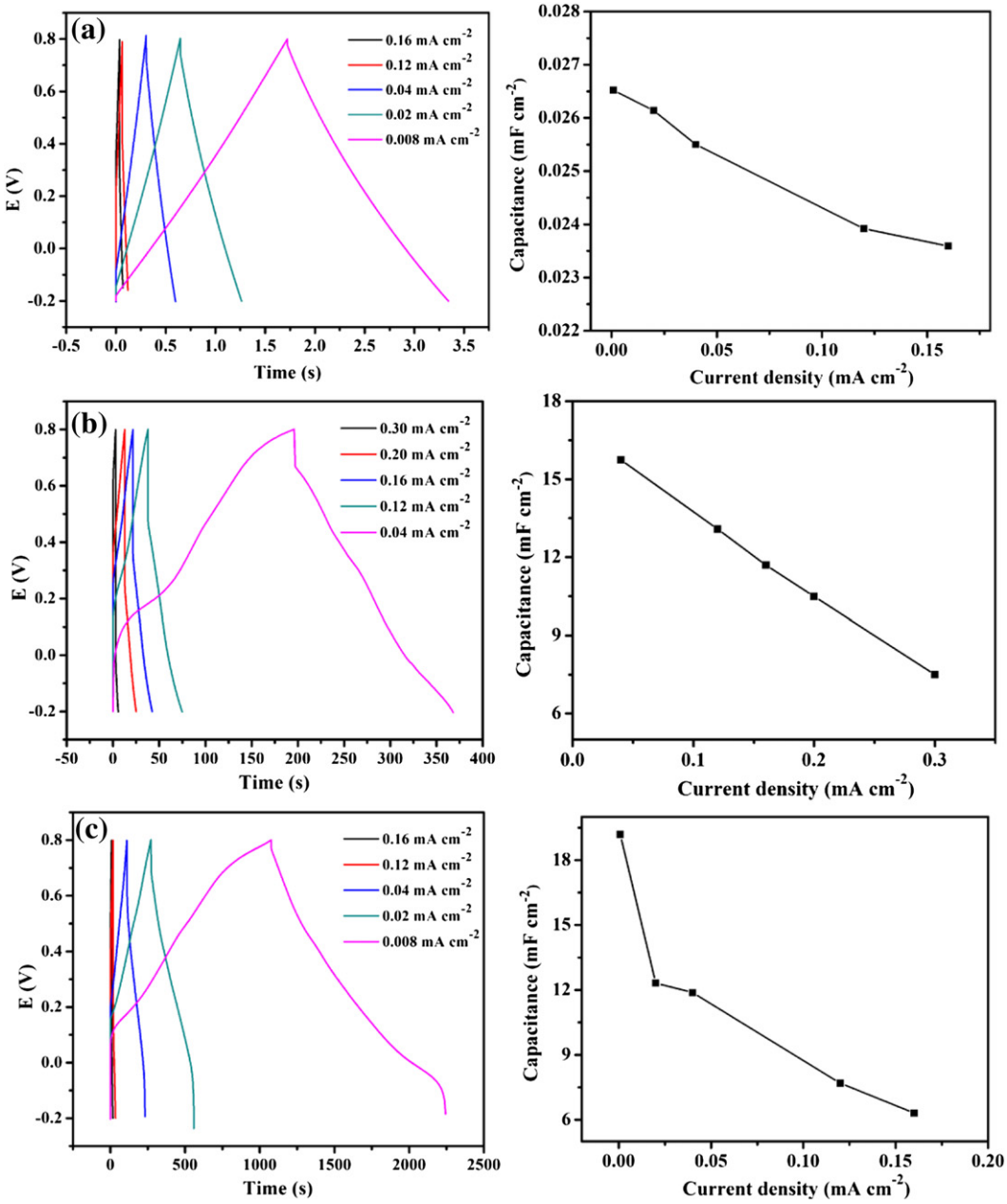

Fig. 12. (a) Charge–discharge curves (left) and current density dependent areal capacitance (right) of the (a) GO film, (b) PANI film, and (c) PANI/GO nanocomposite film in 0.5 M H_2SO_4 aqueous solution.

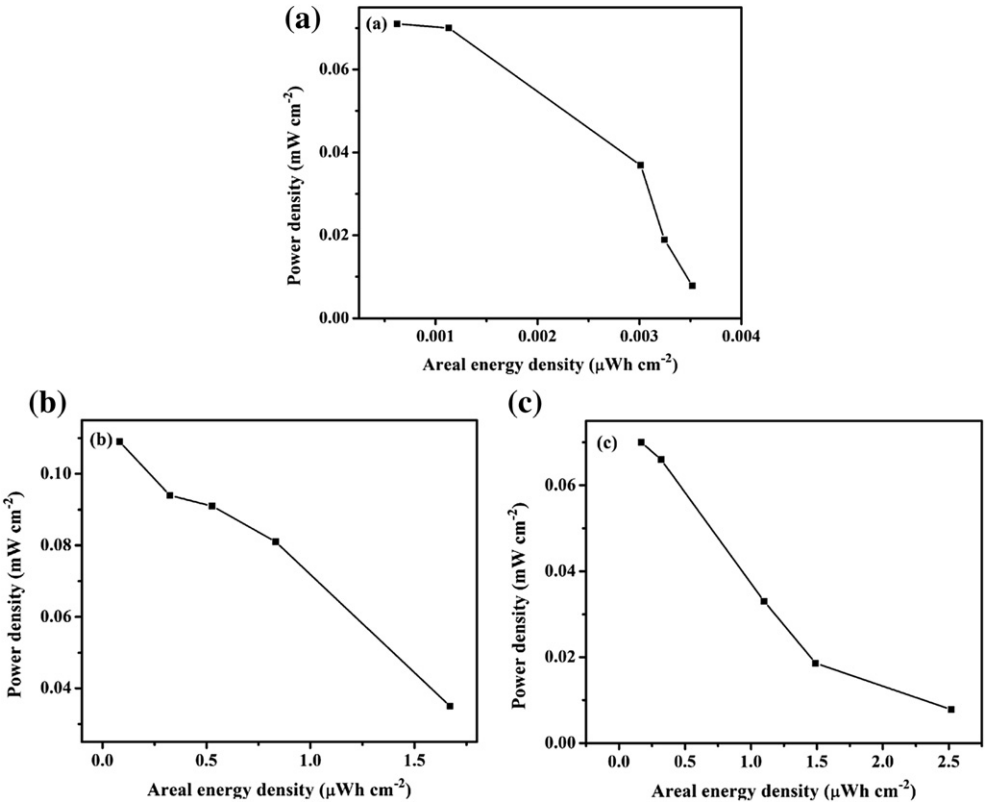

Fig. 13. Areal Ragone plots of the (a) GO film and (b) PANI film, and (c) PANI/GO nanocomposite film.

dependence on the choice of other components including substrates and protective packaging [85]. Therefore, areal energy density and power density of the films are plotted using Equations (8) and (9):

$$E = \frac{\frac{1}{2}C_s\Delta V^2}{3600} \tag{8}$$

$$P = \frac{3600E}{t} \tag{9}$$

where E is the areal energy density in Wh cm^{-2}, P is the areal power density in W cm^{-2}. C_s is the specific capacitance in F cm^{-2}, ΔV is the scanned potential window (excluding IR drop in the beginning of the discharge) in V, t is the discharge time in s. Fig. 13 shows the corresponding Ragone plots based on the area of the films. The PANI/GO film can deliver ~2.52 μWh cm^{-2} in the low power region of ~0.01 mW cm^{-2} and ~0.17 μWh cm^{-2} in the high power region of ~0.07 mW cm^{-2}. Compared to the GO film, the composite film is capable of delivering three orders of magnitude enhanced areal energy density, which is comparable to that of the PANI film, while not sacrificing high areal power densities.

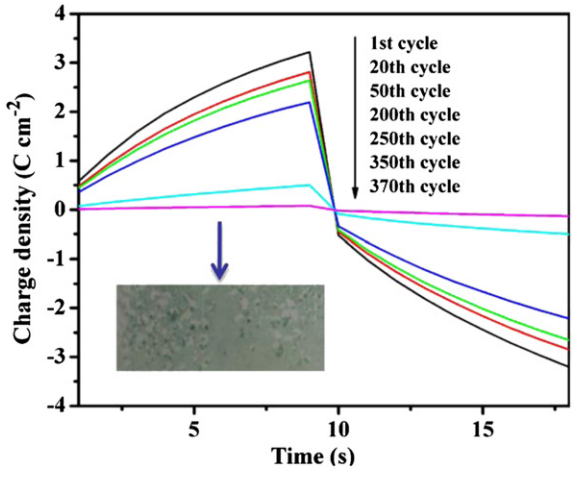

Fig. 14. Charge–discharge cycles for the pure PANI film in 0.5 M H_2SO_4 aqueous solution. The potential step is 0.8 and −0.2 V holding for 10 s, respectively. Inset shows the poor electrochemical stability of the PANI film.

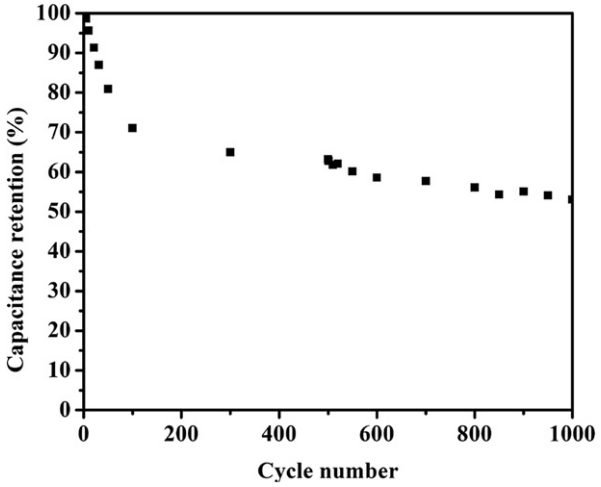

Fig. 15. Capacitance retention of the PANI/GO nanocomposite film as a function of cycling number.

3.5. Stability of PANI/GO composite film

The stability of the capacitors based on CP films, especially for the PANI film during long term cycling is one of their most challenges [86]. No energy storage function existed for the PANI film even after 370 cycles in the charge–discharge cycling, Fig. 14. Compared to the PANI film, the PANI/GO composite film exhibits much higher durability. Fig. 15 shows the capacitance of the PANI/GO composite film during the cycling. The composite film retains 53.1% of the capacitance even after 1000 charge–discharge galvanostatic cycles. The interactions including π–π stacking, electrostatic interactions, and hydrogen bonding existing between GO and PANI [62] prevent the degradation of the polymer matrix due to the shrinking and expanding during the cycling redox reactions [87], therefore in enhancing the stability of the composite film.

4. Conclusions

The PANI/GO nanocomposite films have been prepared by electrodeposition of PANI onto the GO coated ITO glass. The nanocomposite films display multi-color electrochromism at different potentials. A coloration efficiency as high as 59.3 $cm^2\ C^{-1}$ can be obtained. The composite films also possess comparable areal capacitance to that of the pure PANI films at a broad working potential window. The composite films demonstrate a much more enhanced durability than the PANI films during the charge–discharge cycles due to the interactions between the polymer matrix and the GO particles. The PANI/GO nanocomposite films show promising potentials for the electrochromic and energy storage devices applications.

Acknowledgments

The financial supports from Seeded Research Enhancement Grant (REG) and College of Engineering at Lamar University are kindly acknowledged. The support from National Science Foundation-Nanoscale Interdisciplinary Research Team and Materials Processing and Manufacturing (CMMI 10-30755) to obtain DSC and TGA is kindly acknowledged.

References

[1] Simon P, Gogotsi Y. Nat Mater 2008;7:845–54.
[2] Jayalakshmi M, Balasubramanian K. Int J Electrochem Sci 2008;3:1196–217.
[3] Yuan C, Gao B, Shen L, Yang S, Hao L, Lu X, et al. Nanoscale 2011;3:529–45.
[4] Zhang Y, Feng H, Wu X, Wang L, Zhang A, Xia T, et al. Int J Hydrogen Energy 2009;34:4889–99.
[5] Cericola D, Kötz R. Electrochim Acta 2012;72:1–17.
[6] Lee SW, Gallant BM, Byon HR, Hammond PT, Shao-Horn Y. Energy Environ Sci 2011;4:1972–85.
[7] Kötz R, Carlen M. Electrochim Acta 2000;45:2483–98.
[8] Barbieri O, Hahn M, Herzog A, Kötz R. Carbon 2005;43:1303–10.
[9] Tai Z, Yan X, Lang J, Xue Q. J Power Sources 2011;199:373–8.
[10] Shen J, Liu A, Tu Y, Foo G, Yeo C, Chan-Park MB, et al. Energy Environ Sci 2011;4:4220–9.
[11] Korenblit Y, Rose M, Kockrick E, Borchardt L, Kvit A, Kaskel S, et al. ACS Nano 2010;4:1337–44.
[12] Brownson DAC, Kampouris DK, Banks CE. J Power Sources 2011;196:4873–85.
[13] Zhu Y, Murali S, Stoller MD, Ganesh K, Cai W, Ferreira PJ, et al. Science 2011;332:1537–41.
[14] Miller JR, Simon P. Science 2008;321:651–2.
[15] Li J, Cheng X, Shashurin A, Keidar M. Graphene 2012;1:1–13.
[16] Yu G, Hu L, Vosgueritchian M, Wang H, Xie X, McDonough JR, et al. Nano Lett 2011;11:2905–11.
[17] Wu ZS, Wang DW, Ren W, Zhao J, Zhou G, Li F, et al. Adv Funct Mater 2010;20:3595–602.
[18] Brezesinski T, Wang J, Tolbert SH, Dunn B. Nat Mater 2010;9:146–51.
[19] Xia X, Tu J, Zhang Y, Wang X, Gu C, Zhao X, et al. ACS Nano 2012;6:5531–8.
[20] Yang Y, Kim D, Yang M, Schmuki P. Chem Commun 2011;47:7746–8.
[21] Gnanakan SRP, Rajasekhar M, Subramania A. Int J Electrochem Sci 2009;4:1289–301.
[22] Zhu J, Wei S, Zhang L, Mao Y, Ryu J, Mavinakuli P, et al. J Phys Chem C 2010;114:16335–42.
[23] Ding K, Jia H, Wei S, Guo Z. Ind Eng Chem Res 2011;50:7077–82.
[24] Wei H, Yan X, Li Y, Wu S, Wang A, Wei S, et al. J Phys Chem C 2012;116:4500–10.
[25] Wei H, Yan X, Li Y, Gu H, Wu S, Ding K, et al. J Phys Chem C 2012;116:16286–93.
[26] Wei H, Yan X, Wu S, Luo Z, Wei S, Guo Z. J Phys Chem C 2012;116(47):25052–64.
[27] Wang G, Zhang L, Zhang J. Chem Soc Rev 2012;41:797–828.
[28] Liu J, Jiang J, Bosman M, Fan HJ. J Mater Chem 2012;22:2419–26.
[29] Horng YY, Lu YC, Hsu YK, Chen CC, Chen LC, Chen KH. J Power Sources 2010;195:4418–22.
[30] Zotti G, Cattarin S, Comisso N. J Electroanal Chem Interfacial Electrochem 1988;239:387–96.
[31] Liu XX, Zhang L, Li YB, Bian LJ, Su Z, Zhang LJ. J Mater Sci 2005;40:4511–5.
[32] Zhu J, Gu H, Luo Z, Haldolaarachige N, Young DP, Wei S, et al. Langmuir 2012;28:10246–55.
[33] Gu H, Tadakamalla S, Huang Y, Colorado HA, Luo Z, Haldolaarachchige N, et al. ACS Appl Mater Interfaces 2012;4:5613–24.
[34] Osaka T, Nakajima T, Naoi K, Owens BB. J Electrochem Soc 1990;137:2139–42.
[35] Zhou S, Zhang H, Zhao Q, Wang X, Li J, Wang F. Carbon 2012;52:440–50.
[36] Mao L, Zhang K, Chan HSO, Wu J. J Mater Chem 2012;22:80–5.
[37] Watanabe A, Mori K, Iwasaki Y, Nakamura Y, Niizuma S. Macromolecules 1987;20:1793–6.
[38] Silva CHB, Galiote NA, Huguenin F, Teixeira-Neto É, Constantino VRL, Temperini M. J Mater Chem 2012;22:14052–60.
[39] He H, Klinowski J, Forster M, Lerf A. Chem Phys Lett 1998;287:53–6.
[40] Zhu J, Chen M, Qu H, Zhang X, Wei H, Luo Z, et al. Polymer 2012;53:5953–64.
[41] Zhang LL, Zhao S, Tian XN, Zhao X. Langmuir 2010;26:17624–8.
[42] Bora C, Dolui S. Polymer 2012;53:923–32.
[43] Jeong HK, Jin M, Ra EJ, Sheem KY, Han GH, Arepalli S, et al. ACS Nano 2010;4:1162–6.
[44] Hummers WS, Offeman RE. J Am Chem Soc 1958;80:1339.
[45] Kovtyukhova NI, Ollivier PJ, Martin BR, Mallouk TE, Chizhik SA, Buzaneva EV, et al. Chem Mater 1999;11:771–8.
[46] Buron C, Lakard B, Monnin A, Moutarlier V, Lakard S. Synth Met 2011;161:2162–9.
[47] León-Silva U, Nicho M, Hu H, Cruz-Silva R. Sol Energy Mater Sol Cells 2007;91:1444–8.
[48] Hong SY, Park SM. J Phys Chem B 2005;109:9305–10.
[49] Plesu N, Kellenberger A, Mihali M, Vaszilcsin N. J Non-Cryst Solids 2010;356:1081–8.
[50] Cui SY, Park SM. Synth Met 1999;105:91–8.
[51] Peng C, Hu D, Chen GZ. Chem Commun 2011;47:4105–7.
[52] Elkais AR, Gvozdenović MM, Jugović BZ, Stevanović JS, Nikolić ND, Grgur BN. Prog Org Coat 2011;71:32–5.
[53] Chen GL, Shau SM, Juang TY, Lee RH, Chen CP, Suen SY, et al. Langmuir 2011;27:14563–9.
[54] Zhang WL, Park BJ, Choi HJ. Chem Commun 2010;6:5596–8.
[55] Zhang LL, Zhao S, Tian XN, Zhao XS. Langmuir 2010;26:17624–8.
[56] Feng XM, Li RM, Ma YW, Chen RF, Shi NE, Fan QL, et al. Adv Funct Mater 2011;21:2989–96.
[57] Kellenberger A, Dmitrieva E, Dunsch L. J Phys Chem B 2012;116:4377–85.
[58] El-Said WA, Yea CH, Choi JW, Kwon IK. Thin Solid Films 2009;518:661–7.
[59] Zhu J, Wei S, Zhang L, Mao Y, Ryu J, Haldolaarachchige N, et al. J Mater Chem 2011;21:3952–9.
[60] Li Y, Zhao X, Xu Q, Zhang Q, Chen D. Langmuir 2011;27:6458–63.
[61] Gu H, Huang Y, Zhang X, Wang Q, Zhu J, Shao L, et al. Polymer 2011;53:801–9.
[62] Wang H, Hao Q, Yang X, Lu L, Wang X. ACS Appl Mater Interfaces 2010;2:821–8.
[63] Taylor A, Sinclair H. Proc Phys Soc 1945;57:126.
[64] Deng J, Ding X, Zhang W, Peng Y, Wang J, Long X, et al. Polymer 2002;43:2179–84.
[65] Ramesh P, Bhagyalakshmi S, Sampath S. J Colloid Interface Sci 2004;274:95–102.
[66] Chen GL, Shau SM, Juang TY, Lee RH, Chen CP, Suen SY, et al. Langmuir 2011;27:14563–9.
[67] Rudge A, Davey J, Raistrick I, Gottesfeld S, Ferraris JP. J Power Sources 1994;47:89–107.
[68] Fusalba F, Gouérec P, Villers D, Bélanger D. J Electrochem Soc 2001;148(1):A1–6.
[69] Gao Y, Chen S, Cao D, Wang G, Yin J. J Power Sources 2010;195:1757–60.
[70] Huang W, MacDiarmid A. Polymer 1993;34:1833–45.
[71] Argun AA, Aubert PH, Thompson BC, Schwendeman I, Gaupp CL, Hwang J, et al. Chem Mater 2004;16:4401–12.
[72] Dreyer DR, Park S, Bielawski CW, Ruoff RS. Chem Soc Rev 2010;39:228–40.
[73] Amb CM, Dyer AL, Reynolds JR. Chem Mater 2010;23:397–415.
[74] Barsoukov E, Macdonald JR. Impedance spectroscopy: theory, experiment, and applications. John Wiley and Sons; 2005.
[75] Zhou Y, Qin Z-Y, Li L, Zhang Y, Wei YL, Wang LF, et al. Electrochim Acta 2010;55:3904–8.
[76] Mi H, Zhang X, Ye X, Yang S. J Power Sources 2008;176:403–9.
[77] Wang Y, Shi Z, Huang Y, Ma Y, Wang C, Chen M, et al. J Phys Chem C 2009;113:13103–7.
[78] Stoller MD, Park S, Zhu Y, An J, Ruoff RS. Nano Lett 2008;8:3498–502.
[79] Wu Q, Xu Y, Yao Z, Liu A, Shi G. ACS Nano 2010;4:1963–70.

[80] Niu Z, Luan P, Shao Q, Dong H, Li J, Chen J, et al. Energy Environ Sci 2012;5:8726–33.
[81] Wei Z, Wang K, Wu H, Meng Y, Zhang Y. Energy Environ Sci 2012;5:8384–9.
[82] Wang ZL, Guo R, Li GR, Lu HL, Liu ZQ, Xiao FM, et al. J Mater Chem 2012;22:2401–4.
[83] Broughton J, Brett M. Electrochim Acta 2004;49:4439–46.
[84] Mazeikiene R, Malinauskas A. Eur Polym J 2002;38:1947–52.
[85] Dudney NJ. Electrochem Soc Interface 2008;17:44–8.
[86] Xu J, Wang K, Zu SZ, Han BH, Wei Z. ACS Nano 2010;4:5019–26.
[87] Zhu J, Chen M, Qu H, Luo Z, Wu S, Colorado HA, et al. Energy Environ Sci 2013;6:194–204.